Entrapment of Polysulfides by a Black-Phosphorus-Modified Separator for Lithium–Sulfur Batteries

*Jie Sun, Yongming Sun, Mauro Pasta, Guangmin Zhou, Yuzhang Li, Wei Liu, Feng Xiong, and Yi Cui**

With the increasing demand for high capacity energy storage systems, a considerable amount of effort has recently been focused on the development of the lithium–sulfur (Li–S) battery due to its high theoretical energy density (2567 W h kg^{-1}) and the abundance, non-toxicity, and low cost of sulfur.[1–3] Despite the great promise, successful implementation of the Li–S battery is still hindered by its short cycle life and limited power density. Several problems need to be addressed to enable its practical application. i) The low electrical conductivity of sulfur species, which leads to high overpotentials and low utilization of active materials.[4–6] ii) The diffusion of soluble intermediate polysulfide species into the electrolyte, which causes irreversible loss of active material, low coulombic efficiency, short cycle life, and increases the device impedance over time.[7,8] iii) The large volume change of sulfur cathodes during the charge and discharge processes (up to 80%), which induces stress in the electrode and undermines its structural integrity, leading to the loss of electrical contact with the conductive additives and the detachment from the current collector.[9,10]

To address these issues, extensive research has been devoted to engineering the electrode structure and composition to increase the electrical conductivity and to prevent the polysulfide dissolution by physically and/or chemically trapping the sulfur species within the electrodes. To date, several important strategies for advanced electrode design have been explored such as nanoporous carbon–sulfur composites,[11,12] conductive polymer–sulfur composites,[13] as well as metal oxide and sulfide coating.[14–16] Moreover, various routes for the physical trapping of soluble polysulfides beyond the electrode have been explored, including the insertion of a microporous carbon paper between cathode and separator[17,18] and the modification of separators with a carbon coating layer.[19–29] Although carbon materials have shown promise as sulfur-entrapping host structures,[11,12,17–20] their weak interaction with the polar Li_2S_x undermines their application as polysulfide traps.[12–14]

Here we introduce a new Li–S battery functional separator obtained by depositing sulfur-capturing black-phosphorus (BP) nanoflakes onto a Celgard, commercial polypropylene separator. We show how the combination of both the physical adsorption and chemical bonding between polysulfides and BP results in superior polysulfide-capturing properties and consequently superior capacity retention upon cycling. An in-depth in situ and ex situ characterization is carried out to investigate the nature of the polysulfide–BP interaction and compare it to graphene and other polar polymers.[12,13]

BP is defined as phosphorene layers stacked in puckered sub-planes through weak interlayer van der Waals interactions. In a phosphorene monolayer, each P atom is bonded with two adjacent atoms lying in the same plane and with a third P atom from a different plane.[30] BP is the most thermodynamically stable allotrope of phosphorous.[31,32] Owing to its high ignition point of 490 °C, it is not flammable in ambient air as white phosphorus. In terms of appearance, properties, and structure, BP closely resembles graphite: it is black, flaky, and a good electrical conductor (≈300 S m^{-1}).[32] Moreover, the Li^+ diffusion constant within a phosphorene monolayer (zigzag direction) is estimated to be 10^4 times faster than that on graphene at room temperature.[33] In addition, the bonding energies between P and S containing species ranges from 285 to 442 kJ mol^{-1}, slightly lower than the 485 kJ mol^{-1} of a P—P bond.[34] This suggests that BP can chemically interact with the polysulfides without structurally damaging the phosphorene backbone. Once bonded, the good electrical conductivity and the fast Li-ion diffusion properties of phosphorene layer can "reactivate" the polysulfide species, thus minimizing the capacity loss associated with the active material dissolution. Furthermore, our previous study reveals[30] no volumetric change of black phosphorus for lithiation in the voltage window of 2.6–1.7 V.

Figure 1a shows a schematic representation of a coin cell with a conventional and BP-coated separator. The BP-coated side, facing the sulfur-based cathode electrode, intercepts and binds the polysulfides preventing their diffusion through the polypropylene separator (Figure 1b). The vacuum filtration deposition process (Figure 1c,d) results in an excellent adhesion of BP nanoflakes to the commercial separator, as demonstrated by the folding/unfolding test in Figure 1e,f. Scanning electron microscopy (SEM) images of the Celgard polyethylene separator (Figure S1, Supporting Information) show its typical macroporous (≈100 nm pore diameter) structure. After the BP coating, a uniform and dense layer of BP nanoflakes (≈0.4 mg cm^{-2}) forms on the surface of the separator, covering the nanopores

Dr. J. Sun, Dr. Y. Sun, Dr. G. Zhou, Y. Li, Dr. W. Liu, Dr. F. Xiong, Prof. Y. Cui
Department of Materials Science and Engineering
Stanford University
Stanford, CA 94305, USA
E-mail: yicui@stanford.edu
Prof. M. Pasta
Department of Materials
University of Oxford
16 Parks Road, Oxford OX1 3PH, UK
Prof. Y. Cui
Stanford Institute for Materials and Energy Sciences
SLAC National Accelerator Laboratory
2575 Sand Hill Road, Menlo Park, CA 94025, USA

DOI: 10.1002/adma.201602172

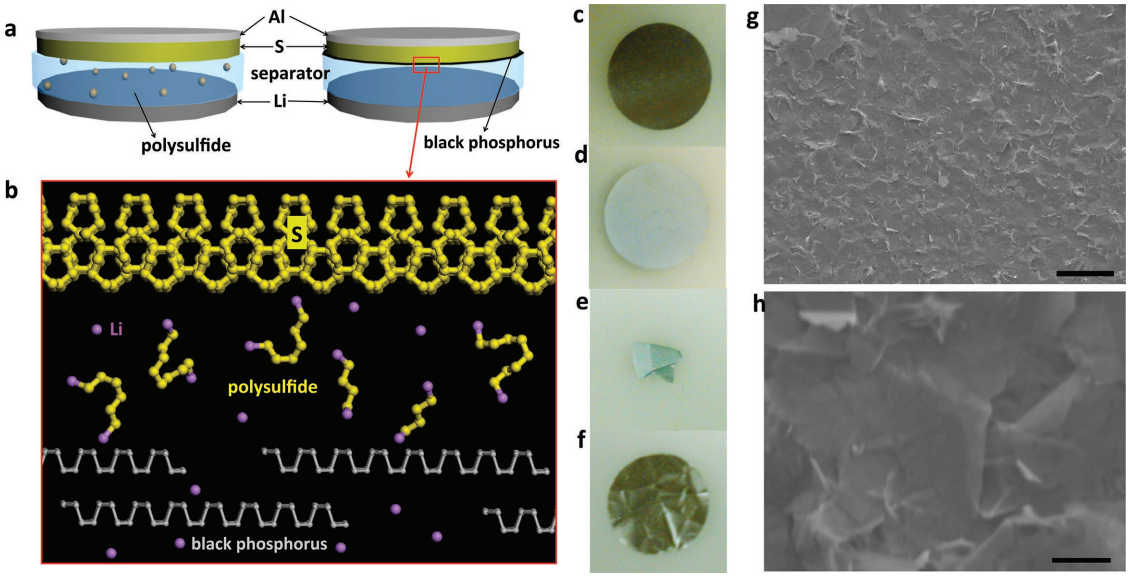

Figure 1. a) Schematic cell configuration of the Li–S cell employing a commercial separator (left) and the BP-coated separator (right). b) Operating principle of the BP coating layer in Li–S battery. Photographs of the as-prepared BP-coated separator: c) cathode-facing side, d) anode-facing side, e) folded, and f) unfolded. g) SEM image of the as-prepared BP-coated separator. h) High-magnification SEM image of the as-prepared BP-coated separator. The scale bars in (g) and (h) are 10 and 1 μm, respectively.

(Figure 1g,h). A detailed characterization of the BP nanoflakes is reported in Figure S2 and S4 in the Supporting Information.

In situ Raman spectroscopy was employed in order to characterize the transition from S_8 to Li_2S during cycling. A prototype Li–S cell for in situ Raman characterization is shown in Figure S5 in the Supporting Information in which a sandwich structure composed of a sulfur cathode coated on aluminum foil, a BP-coated separator, and a lithium metal on copper foil anode was assembled into a transparent pouch cell. The anode and separator were punched with a circular hole in the center with a diameter of 1/20 in. to expose the cathode to the incident laser beam. As shown in **Figure 2**a, the Raman spectra were recorded at five charge states: at open circuit voltage (OCV) 2.42 V (A), 2.10 V (B), 1.70 V (C), 2.39 V (D), and 2.60 V (E) respectively during the first discharge/charge cycle. Figure 2b shows the typical Raman spectra collected from the cathode at different potentials/charge states. It reveals the evolution of the chemical composition on the BP-modified separator surface. At the 2.42 V (A), the peaks at 218 and 470 cm^{-1} can be assigned to those of solid sulfur (S_8).[27] After discharging the cell to 2.1 V (B), the typical features of polysulfides (Li_2S_x, $x = 3–8$)[35,36] can be observed. At 1.7 V (C), the Raman spectrum shows the presence of Li_2S and Li_2S_2.[35] After recharging the cell to 2.39 V (D), the modes of the Li_2S and Li_2S_2 species disappear and only the polysulfides signals can be observed. Further charging to 2.6 V (E), it results in the conversion of polysulfides into S_8.

In order to investigate the efficacy of the BP coating layer for trapping the polysulfides, we performed in situ Raman mapping measurements. The cathode was punched with a circular hole in the center to expose the BP-coated side of the separator to the incident laser beam (Figure 2c and Figure S6, Supporting Information). Raman mapping measurements were recorded at five charge states corresponding to points A to E in Figure 2a. According to the evolution of the sulfur species trapped by BP during the lithiation and delithiation processes, Raman mapping images were collected using different frequency ranges in Figure 2e–i, corresponding to the red square region in the optical microscopy image in Figure 2d. Figure 2e collected at the OCV (point A) with the frequency range 213–227 cm^{-1}, shows no dissolution of the starting material, S_8. At point B (2.1 V), a bright yellow spot appears in Figure 2f, which was collected in the range of 390–403 cm^{-1} and was attributed to the presence of polysulfides. When the cell was discharged to 1.7 V (point C), the bright spot was recorded between 370 and 385 cm^{-1} and corresponds to the formation of Li_2S and Li_2S_2 (Figure 2g). When charging the cell to 2.39 V (D) and 2.6 V (E), the bright spot was converted into polysulfides (Figure 2h) and S_8 (Figure 2i). It is interesting to notice that going from (B) to (E), the distance between the big spot and the smaller one on top was almost unchanged, indicating that the BP coating layer can effectively anchor the various sulfur species thus preventing the diffusion of the polysulfide anions. Moreover, its chemical evolution indicates that sulfur species trapped by the BP layer are electrochemically reactive.

In order to further investigate the interaction between BP and the anchored sulfur species, ex situ X-ray photoelectron spectroscopy (XPS) analysis was carried out. The BP-coated separators retrieved from the cycled cells were washed using 1,2-dimethoxyethane to remove the LiTFSI absorbed on the surface and transferred into the XPS machine via an oxygen-free transfer chamber. **Figure 3**a–c displays a series of XPS spectra of the separators at the same potentials/charge states as the Raman characterization discussed above (Figure 2a). At the OCV (A), only the P $2p_{3/2}$ and P $2p_{1/2}$ signals of BP were recorded (129.9 and 130.7 eV, respectively). At 2.1 V (B), the Li 1*s* and S 2*p* signals can be observed. Three kinds of S 2*p* signals are clearly identifiable: S—S (S $2p_{3/2}$ at 164.1 eV), S—Li (S $2p_{3/2}$ at 161.2 eV), and S—P (S $2p_{3/2}$ at 163.1 eV). According

Adv. Mater. **2016**,
DOI: 10.1002/adma.201602172

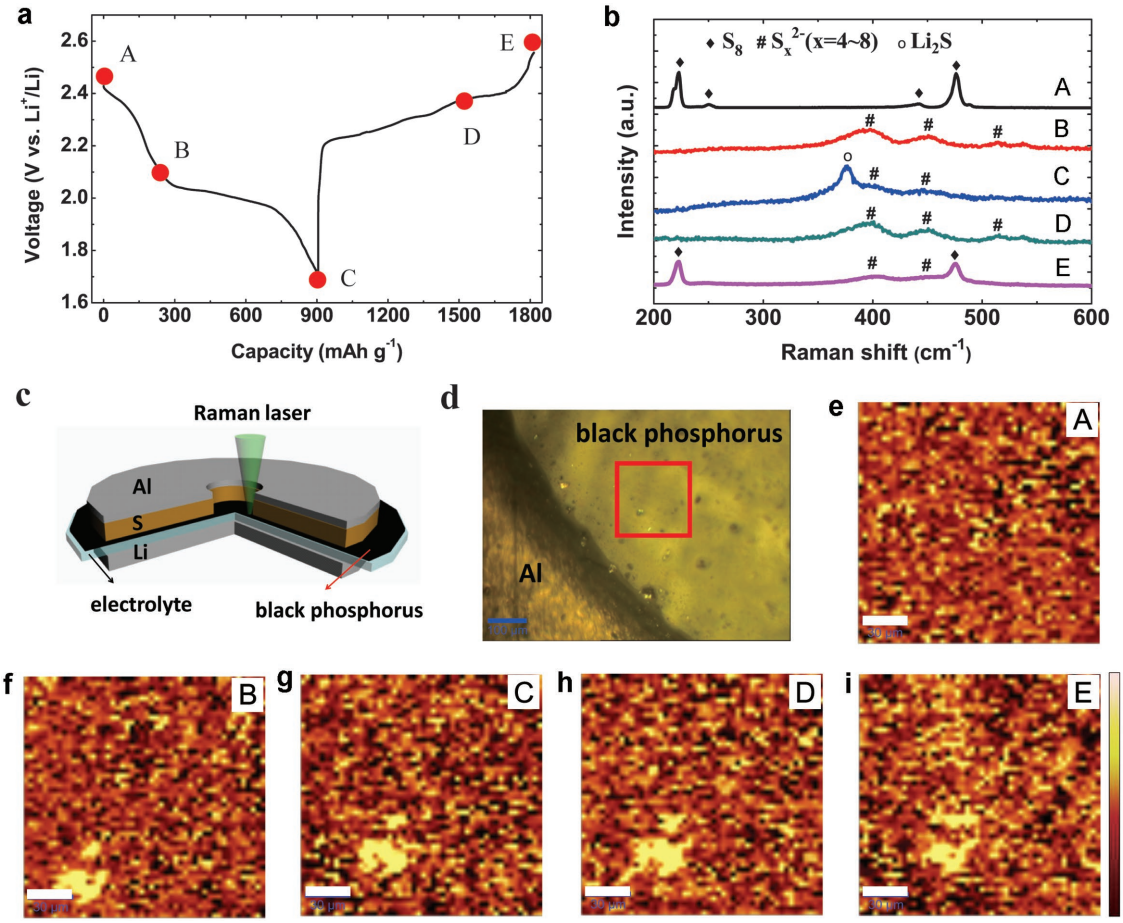

Figure 2. a) First galvanostatic discharge–charge curves of lithium–sulfur cell. b) Corresponding typical Raman spectra of the cathode at five different potentials in (a). c) Schematic of the cross section of Li–S battery with BP-modified separator fabricated in a transparent pouch cell. d) Optical microscopy image of the hole in the aluminum foil. The light yellow region is the coating side of the BP-modified separator. The red square represents the mapping scan region (scale bars, 100 μm). e–i In situ Raman mapping of the selected area at the sub-micrometer scale (red square in (c)) at the potentials corresponding to (A–E) in (a), respectively: collecting e) in the range of 213–227 cm^{-1}; f) in the range of 390–403 cm^{-1}; g) in the range of 370–385 cm^{-1}; h) in the range of 390–403 cm^{-1}; i) in the range of 213–227 cm^{-1}. (Raman mapping scale bars, 30 μm).

to previous reports, the presence of the S—Li bond at this voltage demonstrates the formation of polysulfides.[37] Moreover, three P-related chemical bonds are identifiable: P—P (P $2p_{3/2}$ at 129.9 eV), P—S (P $2p_{3/2}$ at 131.6 eV) and P—Li (P $2p_{3/2}$ at 128.3 eV). These results indicate that the BP interacts with polysulfides via both a P—S and P—Li bonds.

The interaction between BP and polysulfides was investigated by first-principle calculations of the bonding energy between lithium polysulfides/sulfides and the BP surface, at different sulfur loadings. The molecular models of the various lithium polysulfide/sulfide species on BP as well as their binding energies, are reported in Figure 3d. As shown in **Table 1**, the binding energies are in the range 1.32–2.82 eV (without van der Waals interaction), and 1.86–3.05 eV (with van der Waals interaction) and increase with the shortening of the Li_2S_x molecule chains (x, from 8 to 1) due to the weak torsion dystonia. All the binding energies are higher than those on a graphene layer (0.21–0.79 eV),[13] polar polymer molecules (PVP, 1.01–1.29 eV; Triton X-100, 0.66–0.85 eV)[13] and solvents of 1,3-dioxolane/dimethoxyethane (DOL/DME, 0.85 eV).[38] A higher binding energy indicates a more energetically favorable reaction. Therefore, the calculations show how the BP layer (labeled as black, in Figure 3d) strongly adsorbs lithium polysulfide/sulfide species by binding both Li and S atoms. These results are in agreement with the XPS data. In fact, at the end of the lower plateau at 1.7 V, the S $2p$ spectrum (Figure 3b) exhibits an increased proportion of S—Li and the reduced S—S bond, indicating that the lithium polysulfides (Li_2S_x, x = 8–4) transforms into Li_2S_2 and Li_2S. Meanwhile, the increased proportion of S—P bond in S$2p$ spectrum, as well as the increased components of both P—S and P—Li peaks in P$2p$ spectra (Figure 3a), exhibit more P—S and P—Li bonds formed at the surface of BP.

Staircase potential electrochemical impedance spectroscopy[39] was employed to investigate the electrochemical reaction kinetics. The Nyquist plots of the electrochemical impedance spectra (**Figure 4**a–c) were recorded at the potentials of (A), (B), and (C) corresponding to Figure 2a. As shown in Figure 4d–f, the impedance spectra can be modelled with an equivalent circuit consisting of an ohmic resistance of the electrolyte and cell components (R_0) in series with one or more resistance//constant

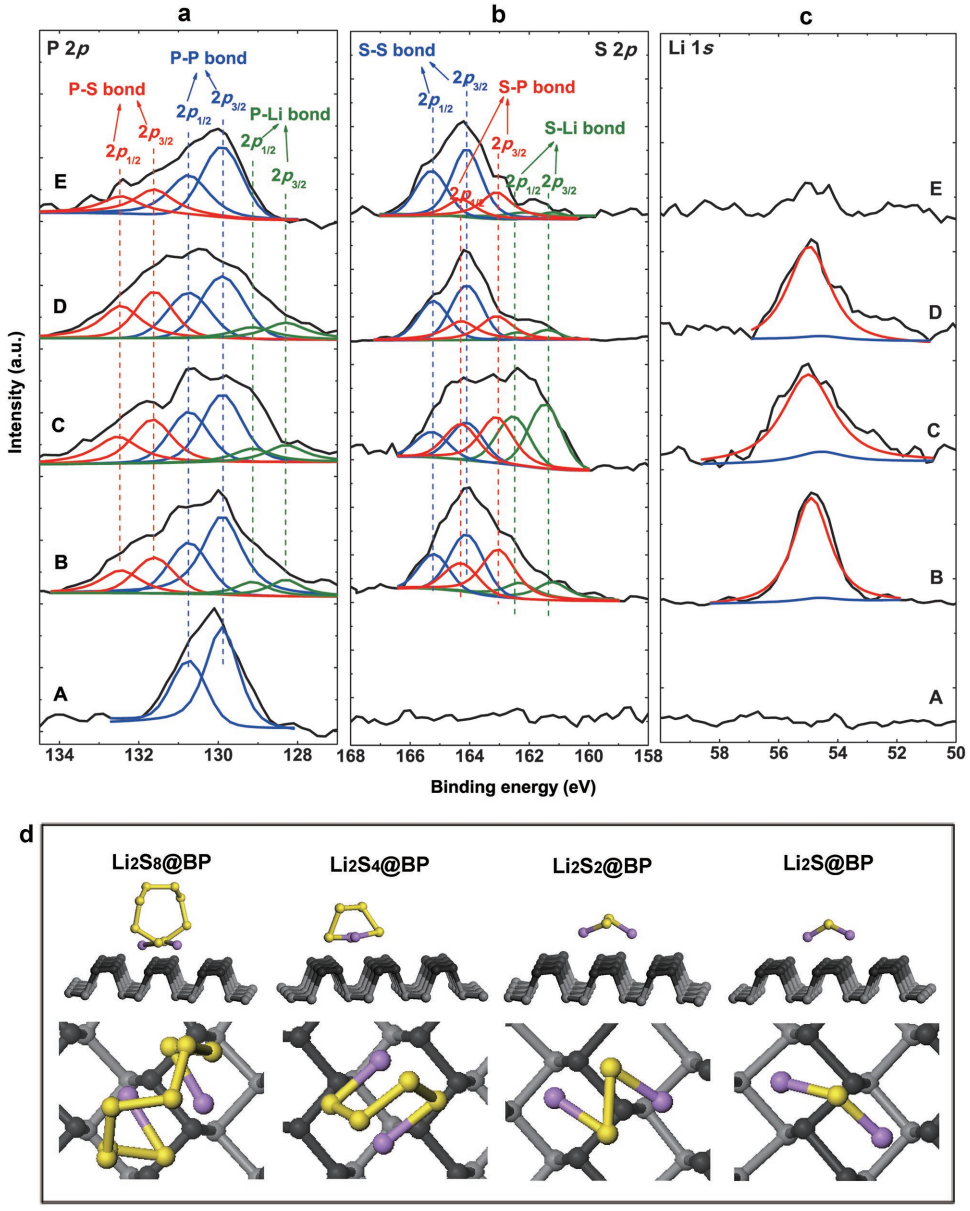

Figure 3. XPS measurements of cycled interlayers and theoretical calculation of molecular binding. a) P 2*p*, b) S 2*p*, and c) Li 1*s* XPS spectra of the BP-modified separators with various depth of discharge and charge at OCV of A) ≈2.4 V, B) 2.1 V, C) 1.7 V, D) 2.39 V, and E) 2.6 V, respectively, according to the first discharge/charge curves of Li–S cell in Figure 2a. ($P2p_{3/2\text{-red}}$(P—S): 131.6 eV; $P2p_{3/2\text{-blue}}$(P—P): 129.9 eV; $P2p_{3/2\text{-green}}$(P—Li): 128.3 eV; $S2p_{3/2\text{-blue}}$(S—S): 164.1 eV; $S2p_{3/2\text{-red}}$(S—P): 163.1 eV; $S2p_{3/2\text{-red}}$(S—Li): 161.2 eV; $Li1s_{red}$(Li—S, Li—P): 55.0 eV; $Li1s_{blue}$(base line).) d) The molecular models of the interaction between BP and Li_2S_8, Li_2S_4, Li_2S_2, and Li_2S calculated via first-principles. The numbers (top line) represent the binding energies in each case. The middle and bottom line show the cross-section and top views, respectively.

phase element (*R*//CPE) elements (*R* and CPE connected in parallel) as well as a Warburg element (W_s).[40,41] A CPE was selected instead of a capacitor because of the non-ideal behavior of the system, reflected as suppressed semicircles in the Nyquist plots.

Table 1. The binding energy of various sulfur species and BP layer with/without van der Waals interaction.

Chemical	Li_2S_8	Li_2S_4	Li_2S_2	Li_2S
Binding energy without vdW [eV]	1.32	1.82	2.01	2.82
Binding energy with vdW [eV]	1.86	2.27	2.33	3.05

At OCV in Figure 4a, the value of ohmic resistance R_0 is 25–30 Ω for the both cells, indicating that the cells have been properly fabricated and tested in the same condition. However, the cell using the conventional separator has only one semicircle, whereas the cell using the BP-modified separator has another small semicircle at middle frequency region. Their equivalent circuits indicate that both of them have charge-transfer resistance at sulfur cathode R_1, while the P-modified cell has an interface contact resistance between BP layer and

Adv. Mater. **2016**,
DOI: 10.1002/adma.201602172

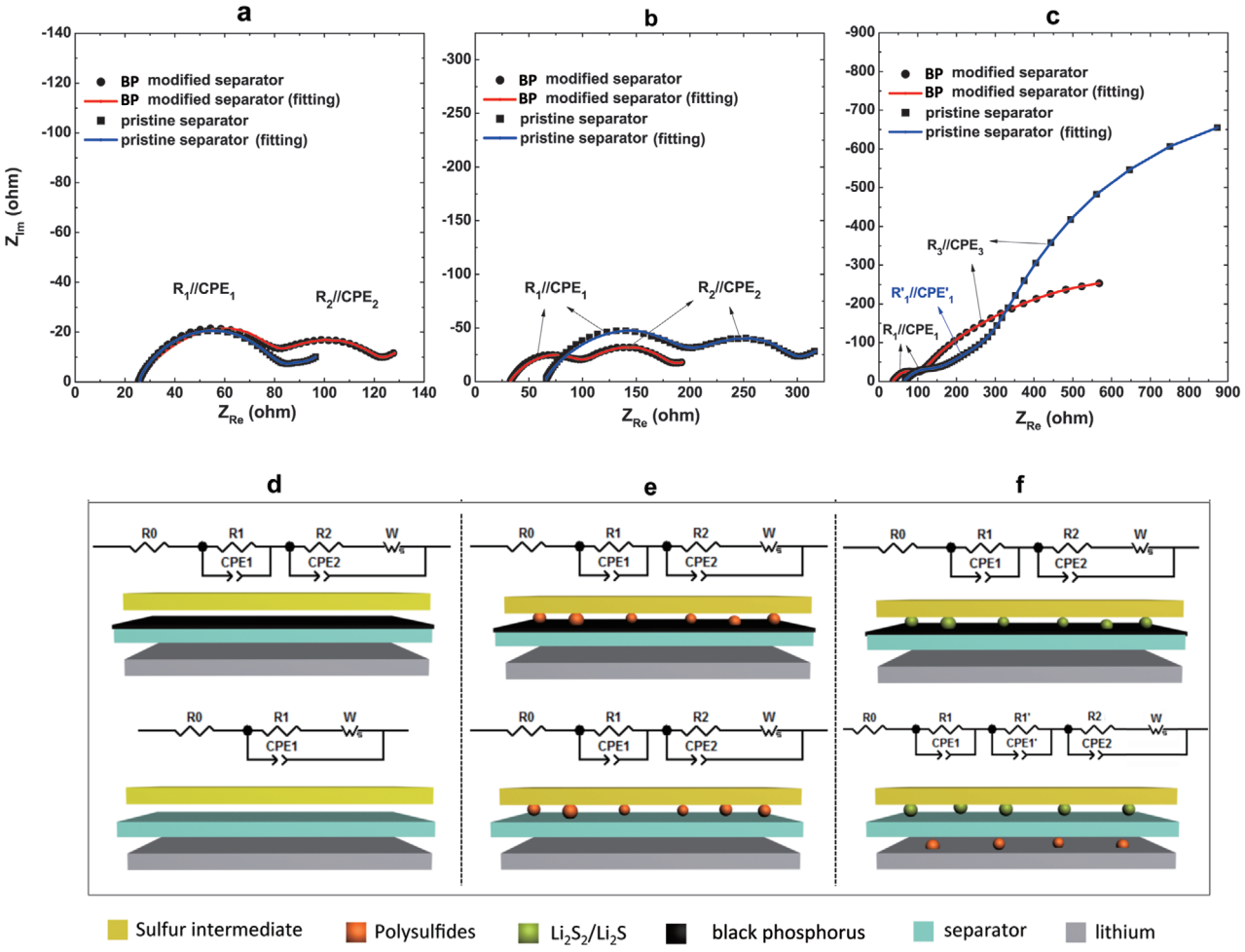

Figure 4. The electrochemical impedance spectra of the Li–S cells using BP-modified and conventional separators, recorded at potentials a) 2.42 V, b) 2.1 V, and c) 1.7 V, respectively, corresponding to the potentials of A, B, and C in Figure 2a. d–f) Equivalent circuits of the Li–S cells using BP-modified (up) and conventional separator (down). (d), (e), and (f) correspond to (a), (b), and (c), respectively.

cathode electrode R_2 resulting in the second semicircle. At 2.1 V in Figure 4b, both of the two cells have two semicircles related to the charge-transfer resistance at the cathode R_1, and the interface contact resistance between soluble polysulfides and cathode electrode R_2, respectively. Both of the R_1 and R_2 from the cell with conventional separator are larger than those in the BP-modified cell. Discharged to 1.7 V in Figure 4c, the second semicircle in the cell with conventional separator increases dramatically, because the polysulfides adsorbed on the separator convert to solid lithium sulfide, leading to a larger interface contact resistance. In addition, for the case of the cell with conventional separator, an additional semicircle presents between R_1//CPE$_1$ and R_2//CPE$_2$, attributed to the immigration of polysulfides onto the anode side (R'_1//CPE$'_1$).

The effect of the BP-modified separator on the electrochemical performance of a Li–S battery is reported in **Figure 5** and compared to a reference cell using a conventional separator and graphene-coated separator, prepared by replacing BP with graphene (same loading). The first galvanostatic discharge–charge curves of the Li–S battery with the different separators at a current density of 0.4 A g^{-1} are shown in Figure 5a. The three cells show typical voltage profiles with two main discharge plateaus at around 2.3 and 2.0 V, attributed to the reactions from solid S_8 to soluble Li_2S_x, and then to solid Li_2S, respectively. The beneficial effect of both coatings is particularly evident on the longer discharge plateau at ≈2.0 V then that in the cell with conventional separator. It indicates that the modified separator inhibits the diffusion of polysulfides to the anode side, and reactivates the polysulfides active. The initial discharge capacity of the BP-modified cell can reach up to 930 mA h g^{-1}, which is 80 mA h g^{-1} higher than the graphene-modified cell, due to the stronger interaction of BP for trapping the sulfur species. In addition, lithium ion can insert/extract into the BP interlayers in the potential range of 1.7–2.6 V (Figure S7, Supporting Information), contributing to an extra capacity. Moreover, for charging process, this Li^+ extraction reaction from BP contributes to a lower overpotential than the other two cells. Figure 5b shows the cycling stability of the cells using the different separators. Comparing to the rapid capacity decay to ≈300 mA h g^{-1} within 40 cycles of the cell using the conventional separator, the BP-modified cell exhibits a capacity of 800 mA h g^{-1} after 100 cycles, corresponding to the retention rate of 86%, much

ADVANCED MATERIALS
www.advmat.de

www.MaterialsViews.com

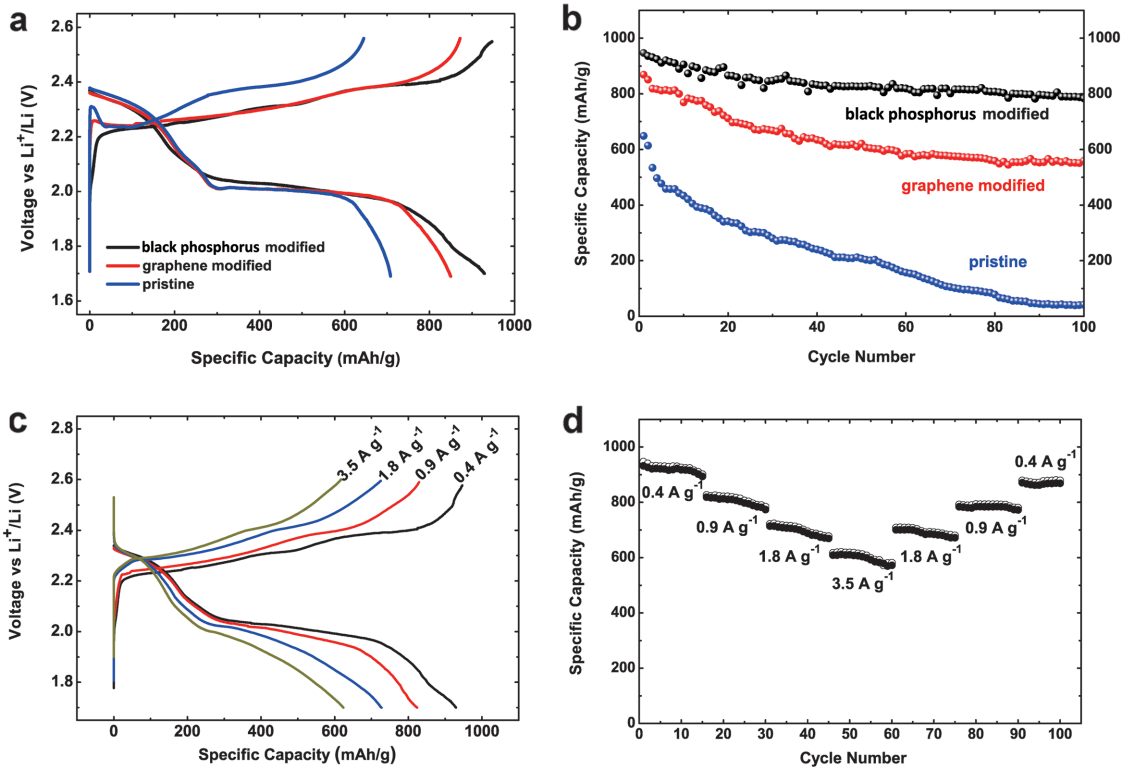

Figure 5. a) First galvanostatic discharge–charge curves of the Li–S battery with BP-modified, graphene-modified and conventional separators, respectively, at a current density of 0.4 A g^{-1}. b) Reversible lithiation capacity and Coulombic efficiency for the first 100 galvanostatic cycles of the three Li–S cells, between 2.6 and 1.7 V at a current density of 0.4 A g^{-1}. c) Galvanostatic discharge–charge curves of the Li–S cell with the BP-modified separator, at different current densities (from 0.4 to 3.5 A g^{-1}). d) Specific capacities of the Li–S cell using BP-modified separator, cycled at various rates.

higher than the graphene-modified cell (66% retention). The high rate cycling performance of the BP-modified cell was further studied in Figure 5c,d. When the current rate was increased to 0.9 A g^{-1}, it could still deliver a reversible capacity of 820 mA h g^{-1}. Even at the very high rates of 1.8 and 3.5 A g^{-1}, the electrode retained a specific capacity of 725 mA h g^{-1} (77%) and 623 mA h g^{-1} (66%), respectively.

In summary, a uniform BP coating layer, with high electron conductivity and ultrahigh Li diffusivity, was introduced on to a commercial polypropylene separator to trap and activate the soluble polysulfides in Li–S batteries. With such a functional composite separator, much increased specific capacity and improved cyclability are achieved for the sulfur electrode with a high sulfur content of 80%. This rational design was proposed based on the investigation of the polysulfides accommodated in the separator. The large surface area of the conducting coating, as well as the strong bonding with both of Li and S atoms, increased the utilization of the polysulfides accommodated in the separator. We showed that the Li–S battery performance was significantly improved with this conducting layer on the separators, indicating that BP can open new avenues to improve the performance of Li–S batteries.

Experimental Section

Experimental methods can be found in the Supporting Information.

Supporting Information

Supporting Information is available from the Wiley Online Library or from the author.

Acknowledgements

This work was supported by the Department of Energy, Office of Basic Energy Sciences, Division of Materials Sciences and Engineering, under contract DE-AC02-76SF00515.

Received: April 24, 2016
Revised: August 8, 2016
Published online:

[1] N. Li, Z. Weng, Y. Wang, F. Li, H.-M. Cheng, H. Zhou, *Energy Environ. Sci.* **2014**, *7*, 3307.
[2] P. G. Bruce, S. a. Freunberger, L. J. Hardwick, J.-M. Tarascon, *Nat. Mater.* **2011**, *11*, 172.
[3] D. Bresser, S. Passerini, B. Scrosati, *Chem. Commun.* **2013**, *49*, 10545.
[4] J. Shim, K. a. Striebel, E. J. Cairns, *J. Electrochem. Soc.* **2002**, *149*, A1321.
[5] Y. V. Mikhaylik, J. R. Akridge, *J. Electrochem. Soc.* **2004**, *151*, A1969.
[6] H. Yao, G. Zheng, P.-C. Hsu, D. Kong, J. J. Cha, W. Li, Z. W. Seh, M. T. McDowell, K. Yan, Z. Liang, V. K. Narasimhan, Y. Cui, *Nat. Commun.* **2014**, *5*, 3943.

DOI: 10.1002/adma.201602172

[7] G. Zhou, S. Pei, L. Li, D.-W. Wang, S. Wang, K. Huang, L.-C. Yin, F. Li, H.-M. Cheng, *Adv. Mater.* **2014**, *26*, 625.
[8] L. Xiao, Y. Cao, J. Xiao, B. Schwenzer, M. H. Engelhard, L. V. Saraf, Z. Nie, G. J. Exarhos, J. Liu, *Adv. Mater.* **2012**, *24*, 1176.
[9] Y. Yang, G. Zheng, Y. Cui, *Chem. Soc. Rev.* **2013**, *42*, 3018.
[10] Z. Wei Seh, W. Li, J. J. Cha, G. Zheng, Y. Yang, M. T. McDowell, P.-C. Hsu, Y. Cui, *Nat. Commun.* **2013**, *4*, 1331.
[11] X. Ji, K. T. Lee, L. F. Nazar, *Nat. Mater.* **2009**, *8*, 500.
[12] Z. W. Seh, H. Wang, N. Liu, G. Zheng, W. Li, H. Yao, Y. Cui, *Chem. Sci.* **2014**, *5*, 1396.
[13] G. Zheng, Q. Zhang, J. J. Cha, Y. Yang, W. Li, Z. W. Seh, Y. Cui, *Nano Lett.* **2013**, *13*, 1265.
[14] Q. Zhang, Y. Wang, Z. W. Seh, Z. Fu, R. Zhang, Y. Cui, *Nano Lett.* **2015**, *15*, 3780.
[15] X. Tao, J. Wang, Z. Ying, Q. Cai, G. Zheng, Y. Gan, H. Huang, Y. Xia, C. Liang, W. Zhang, Y. Cui, *Nano Lett.* **2014**, *14*, 5288.
[16] Z. W. Seh, J. H. Yu, W. Li, P.-C. Hsu, H. Wang, Y. Sun, H. Yao, Q. Zhang, Y. Cui, *Nat. Commun.* **2014**, *5*, 5017.
[17] Y.-S. Su, A. Manthiram, *Nat. Commun.* **2012**, *3*, 1166.
[18] Y.-S. Su, A. Manthiram, *Chem. Commun.* **2012**, *48*, 8817.
[19] S. Chung, A. Manthiram, *J. Phys. Chem. Lett.* **2014**, *5*, 1978.
[20] X. Wang, Z. Wang, L. Chen, *J. Power Sources* **2013**, *242*, 65.
[21] X. Han, Y. Xu, X. Chen, Y.-C. Chen, N. Weadock, J. Wan, H. Zhu, Y. Liu, H. Li, G. Rubloff, C. Wang, L. Hu, *Nano Energy* **2013**, *2*, 1197.
[22] H.-J. Peng, D.-W. Wang, J.-Q. Huang, X.-B. Cheng, Z. Yuan, F. Wei, Q. Zhang, *Adv. Sci.* **2016**, *3*, 1500268.
[23] S. Rehman, S. Guo, Y. Hou, *Adv. Mater.* **2016**, *28*, 3167.
[24] G. Zhou, L. Li, D. W. Wang, X. Y. Shan, S. Pei, F. Li, H. M. Cheng, *Adv. Mater.* **2015**, *27*, 641.
[25] J.-Q. Huang, Q. Zhang, H.-J. Peng, X.-Y. Liu, W.-Z. Qian, F. Wei, *Energy Environ. Sci.* **2014**, *7*, 347.
[26] X. Zhou, Q. Liao, J. Tang, T. Bai, F. Chen, J. Yang, *J. Electroanal. Chem.* **2016**, *768*, 55.
[27] J. Balach, H. K. Singh, S. Gomoll, T. Jaumann, M. Klose, S. Oswald, M. Richter, J. Eckert, L. Giebeler, *ACS Appl. Mater. Interfaces* **2016**, *8*, 14586.
[28] Z. Zhang, G. Wang, Y. Lai, J. Li, Z. Zhang, W. Chen, *J. Power Sources* **2015**, *300*, 157.
[29] U. Stoeck, J. Balach, M. Klose, D. Wadewitz, E. Ahrens, J. Eckert, L. Giebeler, *J. Power Sources* **2016**, *309*, 76.
[30] J. Sun, H.-W. Lee, M. Pasta, H. Yuan, G. Zheng, Y. Sun, Y. Li, Y. Cui, *Nat. Nanotechnol.* **2015**, *10*, 980.
[31] J. Sun, H.-W. Lee, M. Pasta, Y. Sun, W. Liu, Y. Li, H. R. Lee, N. Liu, Y. Cui, *Energy Storage Mater.* **2016**, *4*, 130.
[32] J. Sun, G. Zheng, H. W. Lee, N. Liu, H. Wang, H. Yao, W. Yang, Y. Cui, *Nano Lett.* **2014**, *14*, 4573.
[33] W. Li, Y. Yang, G. Zhang, Y.-W. Zhang, *Nano Lett.* **2015**, *15*, 1691.
[34] Y.-R. Luo, *Comprehensive Handbook of Chemical Bond Energies*, CRC Press, Boca Raton, FL, USA **2007**.
[35] H. Yao, K. Yan, W. Li, G. Zheng, D. Kong, Z. W. Seh, V. K. Narasimhan, Z. Liang, Y. Cui, *Energy Environ. Sci.* **2014**, *7*, 3381.
[36] M. Hagen, P. Schiffels, M. Hammer, S. Dorfler, J. Tubke, M. J. Hoffmann, H. Althues, S. Kaskel, *J. Electrochem. Soc.* **2013**, *160*, A1205.
[37] Y. S. Su, Y. Fu, T. Cochell, A. Manthiram, *Nat. Commun.* **2013**, *4*, 2985.
[38] B. Wang, S. M. Alhassan, S. T. Pantelides, *Phys. Rev. Appl.* **2014**, *2*, 034004.
[39] H. Chen, Q. Zou, Z. Liang, H. Liu, Q. Li, Y. Lu, *Nat. Commun.* **2015**, *6*, 5877.
[40] L. Yuan, X. Qiu, L. Chen, W. Zhu, *J. Power Sources* **2009**, *189*, 127.
[41] N. a. Cañas, K. Hirose, B. Pascucci, N. Wagner, K. A. Friedrich, R. Hiesgen, *Electrochim. Acta* **2013**, *97*, 42.